Contents lists available at www.sciencedirect.com

Journal of Molecular Biology

Lipid-Mediated Folding/Unfolding of Phospholamban as a Regulatory Mechanism for the Sarcoplasmic Reticulum Ca^{2+}-ATPase

Martin Gustavsson[1], Nathaniel J. Traaseth[1], Christine B. Karim[1], Elizabeth L. Lockamy[1], David D. Thomas[1] and Gianluigi Veglia[1,2]*

[1]*Department of Biochemistry, Molecular Biology and Biophysics, University of Minnesota, Minneapolis, MN 55455, USA*
[2]*Department of Chemistry, University of Minnesota, Minneapolis, MN 55455, USA*

The integral membrane protein complex between phospholamban (PLN) and sarcoplasmic reticulum Ca^{2+}-ATPase (SERCA) regulates cardiac contractility. In the unphosphorylated form, PLN binds SERCA and inhibits Ca^{2+} flux. Upon phosphorylation of PLN at Ser16, the inhibitory effect is reversed. Although structural details on both proteins are emerging from X-ray crystallography, cryo-electron microscopy, and NMR studies, the molecular mechanisms of their interactions and regulatory process are still lacking. It has been speculated that SERCA regulation depends on PLN structural transitions (order to disorder, i.e., folding/unfolding). Here, we investigated PLN conformational changes upon chemical unfolding by a combination of electron paramagnetic resonance and NMR spectroscopies, revealing that the conformational transitions involve mostly the cytoplasmic regions, with two concomitant phenomena: (1) membrane binding and folding of the amphipathic domain Ia and (2) folding/unfolding of the juxtamembrane domain Ib of PLN. Analysis of phosphorylated and unphosphorylated PLN with two phosphomimetic mutants of PLN (S16E and S16D) shows that the population of an unfolded state in domains Ia and Ib (T′ state) is linearly correlated to the extent of SERCA inhibition measured by activity assays. Inhibition of SERCA is carried out by the folded ground state (T state) of the protein (PLN), while the relief of inhibition involves promotion of PLN to excited conformational states (Ser16 phosphorylated PLN). We propose that PLN population shifts (folding/unfolding) are a key regulatory mechanism for SERCA.

Corresponding author. Department of Biochemistry, Molecular Biology and Biophysics, University of Minnesota, 6-155 Jackson Hall, 321 Church Street SE, Minneapolis, MN 55455, USA. E-mail address: vegli001@umn.edu.

Abbreviations used: PLN, phospholamban; SERCA, sarcoplasmic reticulum Ca^{2+}-ATPase; EPR, electron paramagnetic resonance; SR, sarcoplasmic reticulum; LOF, loss of function; Gdn HCl, guanidine hydrochloride; DOPC:DOPE, 1,2-dioleoyl-*sn*-glycero-3-phosphocholine:1,2-dioleoyl-*sn*-glycero-3-phosphoethanolamine; DPC, dodecylphosphocholine; TOAC, 2,2,6,6-tetramethyl-piperidine-1-oxyl-4-amino-4-carboxylic acid; HSQC, heteronuclear single quantum coherence; NOE, nuclear Overhauser effect; SEA-CLEANEX, solvent exposed amides-CLEAN chemical exchange; PKA, protein kinase A; CSI, chemical shift index; HNNOE, heteronuclear NOE.

Introduction

Phospholamban (PLN) is a 52-residue integral membrane protein embedded in the sarcoplasmic reticulum (SR) membrane of cardiac muscle[1] that reversibly inhibits the SR Ca^{2+}-ATPase (SERCA), which regulates calcium flux and muscle contractility.[1–4]

Although several X-ray crystallography and cryo-electron microscopy studies focused on SERCA have revealed important details on calcium translocation,[5–9] structural data on the SERCA/PLN complex[10–13] are sparse and do not offer mechanistic details on the regulatory function of PLN.

In the SR membrane, PLN exists as a homopentamer in equilibrium with monomers that bind SERCA.[1,2,4,14] Both the monomer and the pentamer adopt an L-shaped topology, with a cytoplasmic α-helix (domain Ia; residues 1–16) connected to a membrane-spanning α-helix (residues 23–52) by a short loop (residues 17–22).[15–17] The membrane-spanning helix has two dynamically distinct domains: domain Ib (residues 23–30) that is positioned at the hydrophilic portion of the lipid bilayer and domain II (residues 31–52) that exists in the hydrophobic interior.[15,18,19]

Previously, using NMR and electron paramagnetic resonance (EPR) spectroscopies, we detected a conformational equilibrium between two major states: an ordered T state and a disordered R state.[20,21] According to EPR, the R-state population is ∼16% (T state, ∼84%) in the absence of SERCA[22] and becomes slightly more populated in the presence of the enzyme.[21] We then speculated that the regulation of SERCA by PLN occurs via conformational transitions between the T and R states. This hypothesis was supported by our studies on the structural effects of PLN phosphorylation at Ser16[23,24] and by NMR and functional studies of PLN reconstituted in different lipid mimetics.[25–27] In fact, phosphorylation of PLN at Ser16 by protein kinase A (PKA) relieves SERCA inhibition, allowing for more efficient muscle relaxation.[1–3,28] We found that, structurally and dynamically, phosphorylation causes an *order-to-disorder* transition, with an unwinding of domain Ia at residues 14–16 around the phosphorylation site.[16,21,23,24] As a result, the phosphoryl transfer shifts the PLN conformational equilibrium, increasing the R-state population.[21] The latter can be exploited for the design of mutants to control SERCA function.[29] It is also possible to rationalize the effects of phosphomimetic mutations (S16E)[29] used in gene therapy.[30] Although we established the foundations for a rational design of mutants and showed that the excited states of PLN are important for SERCA inhibition,[29] we did not provide a quantitative interpretation of the conformational transitions of PLN between the ground and excited states or elucidate the structural and dynamic features of the excited conformations.

Here, we used EPR and NMR spectroscopies in conjunction with biological activity assays to define the nature of PLN excited states and, at the same time, to establish a quantitative correlation between the population of the excited state and the extent of SERCA inhibition. We show that the conformational equilibrium of PLN is more complex than previously anticipated. We present a new model for the PLN conformational pre-equilibrium and show a linear correlation between the loss of function (LOF) character of PLN phosphomimetic mutants and their excited-state populations.

Results

A four-state model of PLN conformational equilibrium

Based on our previous studies, we hypothesized that PLN undergoes conformational interconversion between two states: a motionally restricted T state with the cytoplasmic domain absorbed on the membrane surface and a more dynamic R state with domain Ia detached from the membrane and mostly unfolded.[20,21,29] To test this hypothesis, we monitored the chemical unfolding of PLN upon addition of guanidine hydrochloride (Gdn HCl) using both EPR in 4:1 DOPC:DOPE (1,2-dioleoyl-*sn*-glycero-3-phosphocholine:1,2-dioleoyl-*sn*-glycero-3-phosphoethanolamine) lipid bilayers and NMR in dodecylphosphocholine (DPC) micelles. We utilized a synthetic (for EPR) or recombinant (for NMR) monomeric variant of PLN (AFA-PLN) that has the same inhibitory power and similar structural topology as wild-type PLN.[18,31]

EPR spectra of TOAC (2,2,6,6-tetramethyl-piperidine-1-oxyl-4-amino-4-carboxylic acid) spin label engineered at position 11 revealed the presence of two resolved peaks: one broad resonance that was assigned to the T state and a sharper peak assigned to the R state (Fig. 1).[22] The R state is very dynamic, with an order parameter threefold lower than the corresponding T state.[21] To follow the chemical unfolding of PLN, we carried out EPR experiments by titrating Gdn HCl into the PLN samples and monitoring the spectral changes of TOAC at positions 11 (domain Ia), 24 (domain Ib), and 36 (domain II). In the absence of chemical denaturant, the populations of the R state were 8% and 28% for positions 11 and 24, respectively; while only the T state was detected at position 36 (Fig. 1). The addition of Gdn HCl caused the disappearance of the TOAC 11 T-state component and a concomitant increase in the peak intensity of the R-state component. This demonstrates a shift in the PLN conformational equilibrium toward the R state for domain Ia. In contrast, the TOAC spectrum for 36
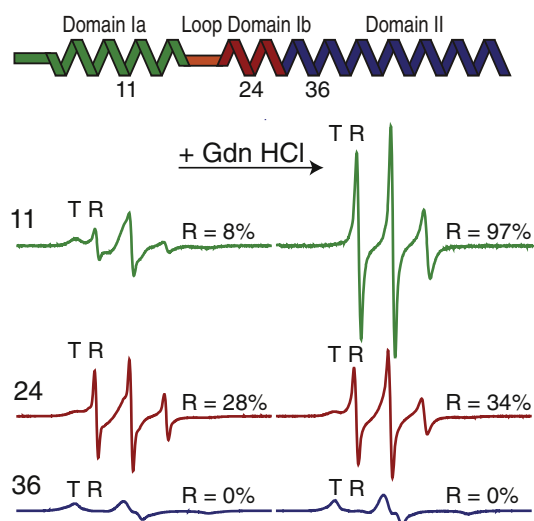
Fig. 1. Chemical unfolding of PLN in lipid vesicles. Continuous-wave EPR spectra of TOAC spin label engineered at positions 11 (domain Ia), 24 (domain Ib), and 36 (domain II). Left: EPR spectra in the absence of Gdn HCl. Right: EPR spectra in the presence of 6 M Gdn HCl (right).

remained unperturbed upon addition of the denaturant and showed that, while domain Ia unfolded completely, the membrane-embedded domain II was still helical in the presence of chemical denaturant. At position 24 (domain Ib), the addition of the Gdn HCl increased the R-state population from 28% to 34%.

To analyze the conformational transitions at the atomic level, we monitored the NMR chemical shifts for both the methyl and the amide groups of PLN upon addition of Gdn HCl using two-dimensional heteronuclear single quantum coherence (HSQC) spectra. As a reference for the unfolded R state of PLN, we used a peptide corresponding to the cytoplasmic residues of PLN (PLN_{1-20}). In aqueous solutions, this peptide is soluble and unfolded, while in the presence of DPC (or lipid vesicles), it is helical and associated with the micelle surface (Supplementary Fig. 1).[32–35]

Titration of Gdn HCl into a PLN sample in DPC micelles caused gradual changes to the chemical shifts for all of the resonances (methyls and amides) in domain Ia, loop, and domain Ib (Figs. 2 and 3). Domain II remained mostly unperturbed with the exception of the C-terminal residues, which is in agreement with the EPR spectra for position 36. The chemical shifts for the PLN methyl groups follow trajectories that are close to linear trajectories (Fig. 3) and at a high concentration of denaturant, overlay with those of PLN_{1-20} without DPC (unfolded R state) (Fig. 4a).

The deviations from linearity, however, are more apparent from the amide chemical shifts. In particular, amide chemical shifts of domain Ia show at

least three different states (see triangulation of chemical shifts for I12), while more linear behavior is observed for resonances located in domain Ib (Fig. 3 and Supplementary Figs. 3 and 4). At high Gdn HCl concentrations, amide chemical shifts in domain Ia overlap with the R state (Fig. 4b). These results demonstrate that, while EPR detects an apparent two-state equilibrium, the conformational states visited by PLN during chemical unfolding are at least three as revealed by NMR spectroscopy. The latter supports the three-state folding model of amphipathic helices proposed by Ladokhin and White and White and Wimley.[36,37] For PLN, the unfolding process highlights three major conformational ensembles: (1) a helical T state, (2) a partially unfolded membrane-associated R′ state, and (3) a totally unfolded membrane-dissociated R state. Note that while the chemical shifts of the methyl groups were sensitive to environmental they only show an apparent two-state equilibrium like the EPR measurements. In contrast, the amide groups are more sensitive to secondary structural changes and therefore are able to detect the presence of the R′ state more clearly.

Interestingly, the plots of the chemical shift changes as a function of the concentration of Gdn HCl show that residues in domains Ia and Ib have
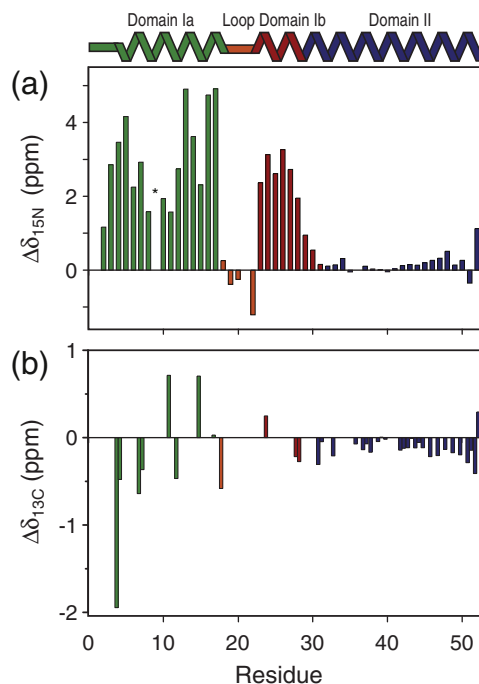

Fig. 2. Chemical shift perturbations of AFA-PLN upon unfolding with Gdn HCl. (a) ^{15}N amide and (b) ^{13}C methyl chemical shift changes as a function of residue. Colors reflect the different structural domains of PLN: domain Ia (green), loop (orange), domain Ib (red), and domain II (blue). The asterisk indicates an overlapped resonance as a result of Gdn HCl unfolding.
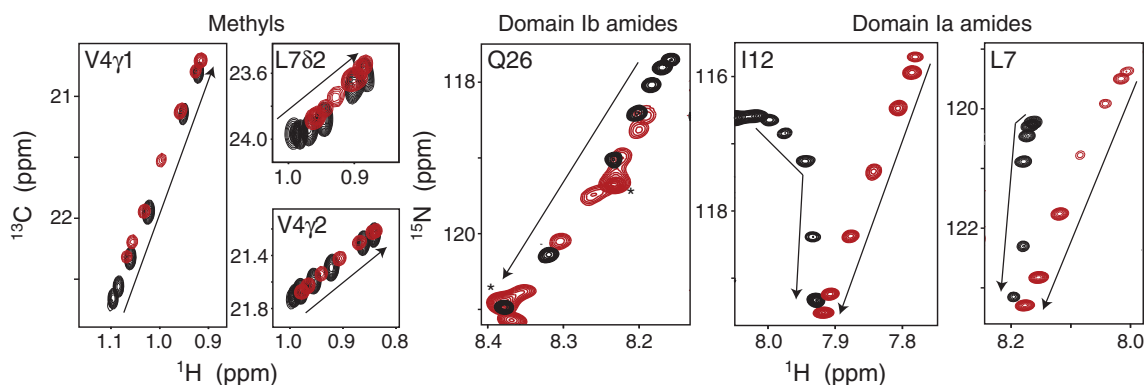
Fig. 3. Chemical unfolding of AFA-PLN and pS16-AFA-PLN. Representative spectra of methyl [^1H,^{13}C] and amide [^1H,^{15}N] HSQC experiments for residues in domain Ia (Val4, Leu7, and Ile12) and domain Ib (Gln26) upon Gdn HCl titration for AFA-PLN (black) and pS16-AFA-PLN (red). AFA-PLN and pS16-AFA-PLN peaks correspond to Gdn HCl concentrations of 0 M, 0.067 M, 0.178 M, 0.48 M, 0.89 M, 1.81 M, and 2.79 M. The direction of the arrows represents the increase in Gdn HCl concentration.

different melting profiles (Fig. 5). Specifically, unfolding curves for residues in domain Ia have a more cooperative unfolding behavior than residues in domain Ib [larger Hill coefficient; 2.2 ± 0.2 *versus* 1.6 ± 0.1 (average ± standard error)] (Supplementary Fig. 5 and Supplementary Table 1). Thus, a lower concentration of Gdn HCl is required to induce unfolding for residues in domain Ib. This behavior is typical of less compact states that are likely to interconvert non-cooperatively.[38,39]

Phosphorylation of PLN at Ser16 causes a complete LOF. This state is responsible for calcium reuptake into the SR membrane and regulates the diastolic phase of the cardiac cycle. Guided by the

EPR data,[21] we originally interpreted phosphorylation of PLN at Ser16 as a shift of the conformational equilibrium toward the R state.[24] To test this, we compared the chemical shifts of both methyl and amide groups with the unfolding experiments carried out in Gdn HCl. While the methyl group chemical shifts of pS16-AFA-PLN are in line with the trajectories toward the unfolded R state, supporting an apparent two-state equilibrium, the amide group chemical shifts do not overlap with those from the Gdn HCl titration. This distinct state (T′ state), which is present in most of the resonances of domain Ia, is partially unfolded as revealed by the ^{13}C chemical shift index (CSI) (Fig. 6)[23,24] but is primarily membrane attached.[23,27] Upon titration with Gdn HCl, the T′ state of phosphorylated PLN is
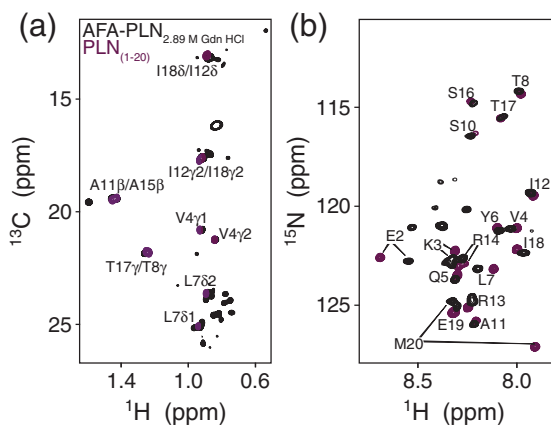

Fig. 4. Methyl and amide fingerprint spectra of PLN$_{1-20}$ and unfolded AFA-PLN. (a) Overlay of [^1H,^{13}C] HSQC spectra of AFA-PLN in the presence of 2.79 M Gdn HCl (black) and PLN$_{1-20}$ in the absence of DPC (purple). (b) Overlay of the [^1H,^{15}N] HSQC spectra for the species reported in (a). With the exception of the terminal residues, the chemical shifts of the resonances of the unfolded domain Ia of AFA-PLN and PLN$_{1-20}$ (in the absence of DPC) are very similar, showing that the PLN$_{1-20}$ free peptide is a good mimic of the R state.
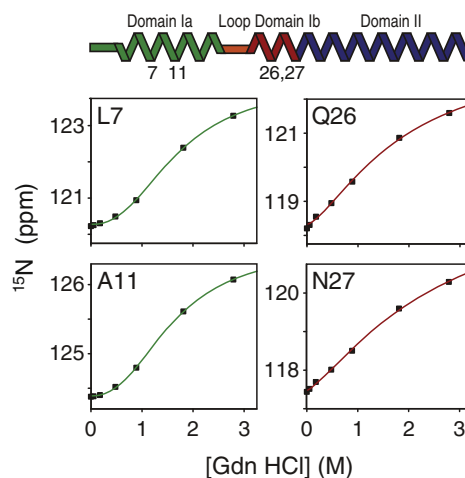

Fig. 5. Unfolding of domains Ia and Ib upon titration of Gdn HCl. Plots of the ^{15}N chemical shifts as a function of Gdn HCl concentration for Leu7 and Ala11 in domain Ia (left) and Gln26 and Asn27 in domain Ib (right). The unfolding of domain Ia is more cooperative than the unfolding of domain Ib.
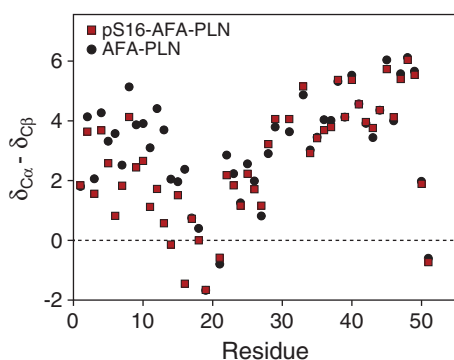
Fig. 6. ^{13}C CSI for AFA-PLN and pS16-AFA-PLN. The CSI is calculated as $^{13}C_{\alpha} - ^{13}C_{\beta} - (^{13}C_{\alpha,RC} - ^{13}C_{\beta,RC})$, where RC stands for the random-coil chemical shifts reported by Zhang *et al.*[40] Consecutive positive CSI values indicate helix propensity.

perturbed toward the unfolded and membrane-detached R state (Fig. 4 and Supplementary Figs. 3 and 4). Note that for most of the resonances the unfolded states of both phosphorylated and unphosphorylated PLN overlap completely. However, slight differences in chemical shifts around the phosphorylation site were observed and were probably due to the charged phosphate group. Also, pS16-AFA-PLN unfolds at significantly lower Gdn HCl concentration than AFA-PLN (average *k* values of 0.7 ± 0.1 and 1.6 ± 0.1) (Supplementary Fig. 6), consistent with the partially unfolded nature of the T′ state.

Based on the above results, we can conclude that the conformational interconversions of PLN include at least four major states for domain Ia and two states for domain Ib. The folding/unfolding equilibrium of domain Ia is dictated by its interactions with the lipids and is regulated by phosphorylation (Fig. 7). The T state can proceed to the R state either through the unfolded and membrane-associated R′ state or through the T′ state. Domain Ib transitions between two states, folded and unfolded, independent of domain Ia.

Pseudo-phosphorylated mutants of PLN and conformational equilibrium

To further test the presence of the excited T′ state, we monitored the effects of phosphomimetic mutations of PLN (S16D and S16E) by monitoring the chemical shifts of both methyl and amide groups. As with the unfolding studies, the methyl group chemical shifts follow an apparent linear trajectory toward the unfolded R state (Fig. 8). In contrast, the amide chemical shifts of the mutants do not fall along the unfolding trajectory for pS16-AFA-PLN or AFA-PLN, rather, they reside in intermediate positions between the resonances of pS16-AFA-PLN and of AFA-PLN. Therefore, it is possible to conclude

that pseudo-phosphorylation and phosphorylation promote a gradual shift in population toward the T′ state, consistent with previous reports that pS16 phosphorylation leads to partial unfolding.[26]

Quantitative correlation between the population of excited state and SERCA inhibition

To investigate a relationship between the population of the excited states and the loss of inhibitory power of PLN, we correlated structure (chemical shifts), dynamics [HX-nuclear Overhauser effect (NOE)] (Supplementary Fig. 9), and water accessibility [solvent exposed amides-CLEAN chemical exchange (SEA-CLEANEX)] (Supplementary Fig. 10) with the extent of PLN inhibition on SERCA's calcium affinity (inhibition; ΔpK_{Ca}) induced by the different mutants. Consistent with previous results,[29] we found the following overall order of increasing inhibition: AFA-PLN→S16E-AFA-PLN→S16D-AFA-PLN→pS16-
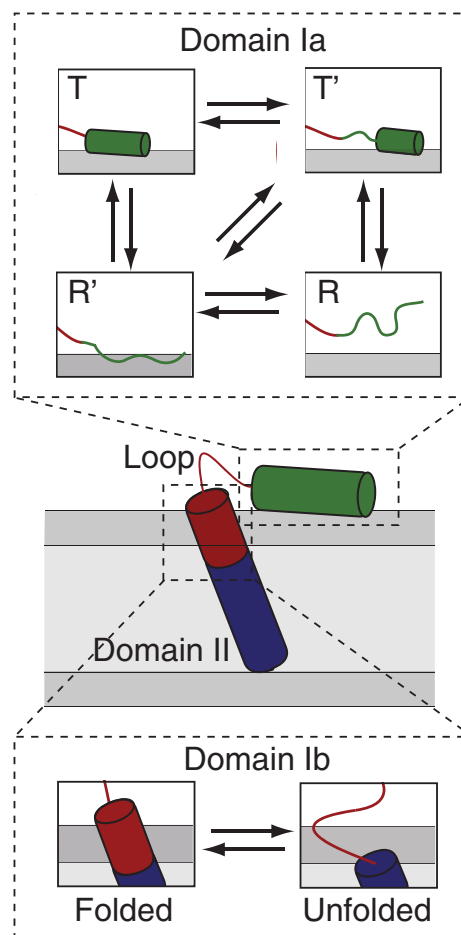

Fig. 7. Model of the conformational equilibrium of PLN. (Top) The T state of domain Ia undergoes unfolding to the R state via an intermediate T′ state or R′ state. (Bottom) Two-state conformational equilibrium for domain Ib.
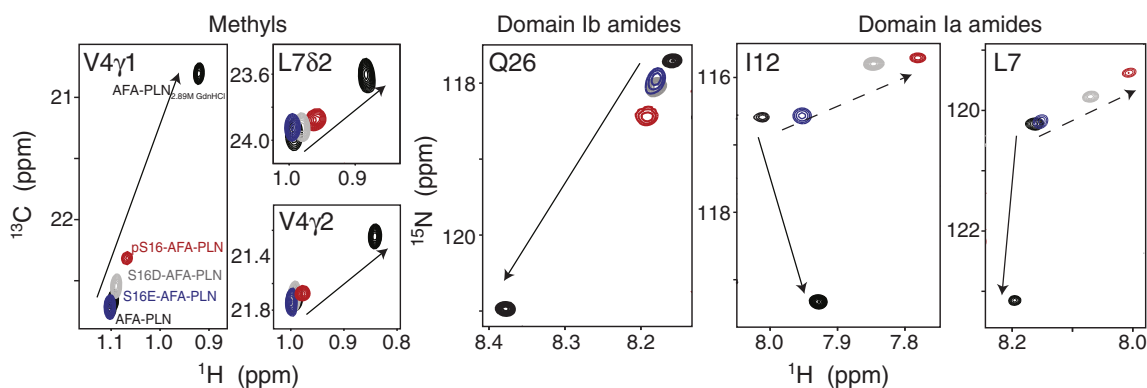
Fig. 8. Methyl and amide HSQC spectra for Ser16 phosphorylated AFA-PLN and the pseudo-phosphorylated variants. [^{1}H,^{13}C] and [^{1}H,^{15}N] HSQC spectra for AFA-PLN (black), S16E-AFA-PLN (blue), S16D-AFA-PLN (gray), and pS16-AFA-PLN (red). The continuous-line arrows point to the AFA-PLN resonance in the presence of Gdn HCl, while the broken-line arrow visually traces the transition from AFA-PLN (T state) to pS16-AFA-PLN (T′ state).

AFA-PLN (Table 1). In order to link the structure to the function, we adopted the approach proposed by Li *et al.*,[41] correlating the average chemical shift change (corresponding to T to T′) for each mutant with the respective SERCA inhibitory potency. The resonances of AFA-PLN were defined to be 100% T state, while those from pS16-AFA-PLN were set to 100% T′ state. The structure–function correlation plot is reported in Fig. 9a. The linearity of this plot (correlation coefficient = 0.98) indicates a direct correlation between the increase in the population of the T′ state and the loss of inhibition. Similar correlations with the inhibitory potency are obtained for both fast dynamics (ps-ns) and solvent accessibility (Fig. 9b and c). This is in agreement with the partially unfolded character of the T′ state, which makes it more dynamic and solvent accessible than the T state and allows it to exchange directly with the completely unfolded R state (Fig. 7). These data suggest that the promotion of PLN from the ground T state to the excited T′ state (and likely R state) results in LOF.

Discussion

Based on our previous investigations,[16] we hypothesized that the conformational equilibrium

Table 1. SERCA inhibition for PLN mutants

PLN variant	ΔpK_{Ca}
AFA-PLN	0.20 ± 0.02
S16E-AFA-PLN	0.14 ± 0.04
S16D-AFA-PLN	0.08 ± 0.04
pS16-AFA-PLN	0.02 ± 0.02

pK_{Ca} values were determined from fits to the Hill equation (see Materials and Methods). Inhibition was measured from the difference in pK_{Ca} in the absence and in the presence of a 10-fold excess of PLN (ΔpK_{Ca}). Standard errors were calculated from the average of three measurements.

of PLN is central to SERCA regulation. However, in our original papers, both EPR and NMR studies revealed the presence of an apparent two-state equilibrium (T and R states).[20,21,42] Here, we provide evidence that PLN has pre-existing equilibria between several conformational states, exemplified by the folding/unfolding of both domain Ia and Ib. For domain Ia methyl groups, the chemical shift trajectories for chemical unfolding follow an apparent two-state equilibrium in agreement with EPR data. In contrast, the trajectories for amide group chemical shifts showed the presence of four conformational states, which is in agreement with the folding model of amphipathic helices.[36,37] On the other hand, for domain Ib, the folding/unfolding process involves a simpler two-state model, as we also found using Carr–Purcell–Meiboom–Gill relaxation dispersion methods.[42] This new, more complex model agrees with recent data from Hughes *et al*. and Abu-Baker and Lorigan,[25,26] who proposed an active role of lipids in modulating PLN structural dynamics and SERCA inhibition. At the same time, it explains previous mutagenesis studies, which identified a number of sites in domain Ia of PLN that lead to relief of SERCA inhibition.[43] Specifically, residues populating the hydrophobic face of the amphipathic domain Ia (V4, L7, and I12) are among these *hot spots*,[43] which are inserted into the lipid bilayer.[17] Shortening the side chain of these residues would likely attenuate the interactions of domain Ia with the membrane environment, supporting the hypothesis that lipid bilayers influence the regulatory process in the context of membrane detachment and helix unfolding. Interestingly, attachment of a lipid anchor to the N-terminus completely shifts PLN to the T state, with Ser16 phosphorylation of this lipidated PLN failing to relieve SERCA inhibition.[21,33] This result also strongly supports the structure–function
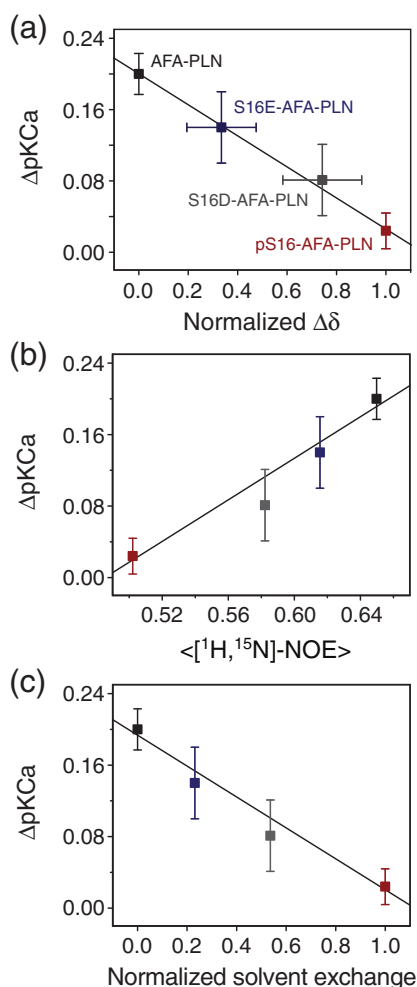
Fig. 9. Structure–dynamics function relationships for AFA-PLN, Ser16 phosphorylated AFA-PLN, and pseudophosphorylated mutants. (a) Correlation between combined ^{15}N-HSQC chemical shift change (normalized $\Delta\delta$), averaged [^{1}H,^{15}N] NOE in domain Ia and the loop (b), and normalized solvent exchange from SEA-CLEANEX experiments (c) with SERCA inhibition from ATPase assays (ΔpK_{Ca}) for AFA-PLN (black), S16E-AFA-PLN (blue), S16D-AFA-PLN (gray), and pS16-AFA-PLN (red). See Materials and Methods for calculation of ΔpK_{Ca}, normalized $\Delta\delta$, $\langle$[^{1}H,^{15}N] NOE$\rangle$, and normalized solvent exchange.

relationship reported in Fig. 9. It is important to stress that the relative population of states can potentially be biased by the choice of membrane mimic. For example, in DPC micelles, the T and T′ states are primarily detected. However, solid-state NMR experiments in dimyristoylphosphatidylcholine lipid bilayers found domain Ia to be predominantly unfolded.[44] This suggests an important role of lipid charge, head groups, and possibly bilayer curvature in influencing the conformational equilibria and extent of aggregation of PLN.

Tuning PLN conformational equilibria leads to the control of SERCA activity. Recently, we showed that to gain complete control over PLN inhibition it is necessary to map the transition to the excited states.[29] Our new data show that pseudo-phosphorylation and phosphorylation of PLN increase the population of T′ state. Since the T′ state exchanges more readily with the fully unfolded R state (Fig. 7), it is likely that the R state also increases in population. The correlation between membrane detachment/unfolding and SERCA inhibition (Fig. 9) suggests that these states need to be considered in the design of new, more efficient LOF PLN mutants. To this extent, the S16D mutation is more similar in structure and dynamics to pS16-AFA-PLN than is the S16E mutant. This is supported by SERCA inhibition assays that show a greater LOF character for S16D-AFA-PLN than for S16E-AFA-PLN and would make the S16D mutant a better candidate for positive inotropic therapy.[45]

An important corollary of this study is the intrinsic flexibility and versatility of the cytoplasmic domain of PLN that when detached from the membrane surface behaves as an intrinsically disordered domain that can adopt several conformations.[46,47] In the heart muscle, PLN interacts with several different partners to elicit its regulatory function. Specifically, PLN associates with the lipid bilayer, SERCA, PKA, Ca^{2+}/calmodulin-dependent protein kinase II, A-kinase anchoring protein 18δ, protein phosphatase 1, HS-1-associated protein X-1, and itself in the form of a pentamer state. How can this protein with such a simple structure and topology bind these diverse biomolecules? We believe that the answer is encoded in its flexibility and malleability (i.e., dynamics) that enable PLN to undergo conformational changes and mold into different binding sites.

Finally, it is worth noting that PLN can be divided into two main regions: an inhibitory transmembrane segment and a cytoplasmic regulatory region. The latter is reminiscent of the autoinhibitory elements found in Vav and light–oxygen–voltage proteins, where an amphipathic helical switch is activated upon phosphorylation or light.[41,48] In the case of Vav and light–oxygen–voltage, this regulatory element is covalently attached to the proteins with the amphipathic helix undergoing folding/unfolding transitions upon interaction with the protein surface. For SERCA, the reversible regulatory element is provided by PLN that is modulated by the folding/unfolding transitions via the lipid bilayer and phosphorylation. Given the high level of similarity between PLN and other single-pass membrane protein subunits such as the FYXD family, it is likely that the mechanism described in this paper is a general one, also found in the regulation of other ion pumps.

Materials and Methods

Purification of PLN protein

Recombinant AFA-PLN, S16D-AFA-PLN, and S16E-AFA-PLN were grown and purified as described by Buck *et al.*[49] PLN$_{1-20}$ was expressed in *Escherichia coli* and was purified as described by Masterson *et al.*[50] To obtain full phosphorylation at Ser16, we dissolved lyophilized AFA-PLN protein at a concentration of 0.3 mg/ml in 20 mM Mops buffer (pH 7.0) containing 1% (w/v) *n*-octyl-β-D-glucopyranoside, ATP (1 mM), and MgCl$_2$ (1 mM).[23] Phosphorylation was accomplished by the addition of purified recombinant PKA[51,52] at a 1:2000 PKA:AFA-PLN molar ratio and was incubated for ~12 h at 30 °C. After purification by reversed-phase HPLC, the pS16-AFA-PLN was lyophilized and stored at −20 °C.

Assay for SERCA activity

For SERCA activity measurements, AFA-PLN, pS16-AFA-PLN, S16E-AFA-PLN, and S16D-AFA-PLN were reconstituted into 4:1 DOPC:DOPE lipid bilayers. SERCA was purified in octaethylene glycol monododecyl ether ($C_{12}E_8$)[5] and was added to the lipid vesicle suspension containing 700:1 lipid:SERCA and 10:1 PLN:SERCA molar ratios. Subsequently, the samples were incubated with Bio-Beads (30:1 Bio-Beads:$C_{12}E_8$ by weight) (Bio-Rad Laboratories) to remove excess detergent. A coupled NADH assay was used to measure SERCA activity (hydrolysis of ATP) at 37 °C as a function of calcium concentration.[53] The rate of enzyme activity was measured as a decrease of NADH absorption at 340 nm using a SpectraMax plate reader (Molecular Devices). Data were fit using the Hill equation to extract the maximum activity (V_{max}), Hill coefficient (n), and calcium concentration needed to achieve half maximal activity (pK_{Ca}).[54]

EPR spectroscopy

For EPR experiments, AFA-PLN with the TOAC spin label substituted at 11, 24, or 36 was synthesized and reconstituted into lipid vesicles containing DOPC:DOPE (4:1, 200 lipids per PLN).[54] EPR spectra were acquired using a Bruker ELEXSYS 500 spectrometer with the SHQ cavity. Samples (20 μl in a 0.6-mm-i.d. quartz capillary) were maintained at 4 °C using the Bruker temperature controller with a quartz Dewar insert. The field modulation frequency was 100 kHz, with a peak-to-peak amplitude of 2 G. The microwave power was 7.9 mW, producing moderate saturation (so that signal intensity was at least 50% of maximum) without a significant effect on the spectral lineshape. EPR spectra were simulated as a sum of one or two components, each component produced by a population having a static random distribution of membrane orientations and undergoing rotational diffusion in a restricting potential (defined by order parameter *S*) with a single rotational correlation time.[21] Experimental spectra were fit by summing simulated components, yielding mole fractions.

NMR spectroscopy

To prepare NMR samples of the AFA-PLN variants, we dissolved lyophilized protein in NMR sample buffer containing 20 mM NaHPO$_4$, 120 mM NaCl, 0.01% NaN$_3$, 5% D$_2$O, 6 M Gdn HCl, 300 mM deuterated DPC, and pH 6.0 uncorrected for isotopic effect. Gdn HCl was subsequently dialyzed against 1 l of NMR sample buffer. This procedure gave more homogenous spectral lines and avoided protein aggregation. All of the NMR experiments were performed on Varian VNMRS and Inova spectrometers operating at a ^{1}H frequency of 600 MHz and at a temperature of 37 °C. Data were processed using NMRPipe[55] and were viewed and analyzed in Sparky.[56] Protein amide fingerprints were analyzed using gradient-enhanced [^{1}H,^{15}N] HSQC experiments.[57] The data were acquired using 1544 complex points in the direct ^{1}H dimension and 50–80 increments in the indirect ^{15}N dimension. Gradient-enhanced constant-time [^{1}H,^{13}C] HSQC experiments were utilized to measure methyl group chemical shifts. For PLN$_{1-20}$ and each AFA-PLN mutant, 8 scans with 2048 complex points and a spectral width of 12,000 Hz in the direct ^{1}H dimension and 64 points with a spectral width of 3500 Hz in the indirect ^{13}C dimension were acquired. After Fourier transformation, the data were zero filled to a final matrix size of 4096 × 2048.

Heteronuclear [^{1}H ^{15}N] steady-state NOE measurements were acquired using the pulse sequence of Farrow *et al.*[58] Two-dimensional spectra with and without a 3-s ^{1}H saturation period were acquired to obtain the ratio between peak intensities in the saturated (I_{sat}) unsaturated (I_{unsat}) spectra:

$$[^1\mathrm{H}, ^{15}\mathrm{N}]\mathrm{NOE} = I_{sat} / I_{unsat} \qquad (1)$$

The uncertainty of the measurement was estimated for each residue from the relationship:[58]

$$\sigma[^1\mathrm{H}, ^{15}\mathrm{N}]\mathrm{NOE} / [^1\mathrm{H}, ^{15}\mathrm{N}]\mathrm{NOE} \qquad (2)$$

$$= \sqrt{\left((\sigma_{sat} / I_{sat})^2 (\sigma_{unsat} / I_{unsat})^2 \right)}$$

where σ_{sat} and σ_{unsat} are the baseline noise in the saturated and unsaturated spectra, and σ_{HNNOE} is the estimated error for the heteronuclear NOE (HN NOE) values.

To measure the solvent exchange for amide protons, we performed [^{1}H,^{15}N] SEA-CLEANEX experiments.[59] This pulse sequence utilizes a spin-echo filter to select for water magnetization followed by a mixing period to allow for exchange between protein and solvent.[60] To eliminate NOE contributions, we implemented the CLEANEX-PM mixing scheme.[61] Four different mixing times (30, 60, 120, and 200 ms) were used to follow the buildup of peaks corresponding to solvent exchanging amide protons. A total of 64–96 scans were recorded with 2048 complex points in the direct ^{1}H dimension and 40 increments in the indirect ^{15}N dimension. Spectral widths were 12,000 Hz and 1200 Hz in the direct and indirect dimensions, respectively. A shifted sine-bell window function was applied to all data sets, which were zero filled to 4096 in both dimensions prior to Fourier transformation.

Gdn-HCl-induced denaturation was done by titrating Gdn HCl from a 6 M stock solution to AFA-PLN at pH 6.0. Six additions were made to a final Gdn HCl concentration of 2.8 M, and [^{1}H,^{15}N] HSQC and [^{1}H,^{13}C] HSQC spectra were acquired after each addition as described above. For the analysis of unfolding, spectra were referenced to 10 mM 2,2-dimethyl-2-silapentane-5-sulfonate, and ^{15}N peak shifts were plotted as a function of Gdn HCl concentration. The data were fit using the Hill equation:

$$\Delta\delta = \frac{(\delta_{end} - \delta_{start})[\text{Gdn HCl}]^n}{[\text{Gdn HCl}]^n + k^n}$$

where n is the Hill coefficient, and k is the unfolding half point. Hill coefficients for residues in domain Ib of PLN (22–28) and domain Ia (3–16) were compared using a t-test. Residue 9 was excluded, since it could not be assigned; residues 2, 29, and 30 were excluded, since those fit poorly to the Hill equation. k values for domain Ia and Ib of AFA-PLN and pS16-AFA-PLN (residues 3–16 and 22–28) were compared with a t-test.

Structure, dynamics, function relationship

Chemical shift changes for the different mutants were calculated according to the expression:

$$\Delta\delta_{combined} = \sqrt{\left((\Delta\delta)^1H\right)^2 + \left(\frac{(\Delta\delta)^{15}N}{5}\right)^2} \qquad (6)$$

where $\Delta\delta_{combined}$ is the difference in chemical shift relative to AFA-PLN. Several resonances within the HSQC spectra (Supplementary Fig. 2) that had a gradual change in chemical shifts from AFA-PLN→S16E-AFA-PLN→S16D-AFA-PLN→pS16-AFA-PLN (Leu7, Thr8, Ala11, Ile12, Ala15, Ile18, Glu19, Gln22, Gln23, Arg25, Gln26, Asn27, Leu28, Gln29, and Asn30) were used in the analysis. Each resonance shift was calculated using the following formula:

$$p = \frac{\omega_{mutant} - \omega_{AFA}}{\omega_{pAFA} - \omega_{AFA}} \qquad (7)$$

where ω is the combined chemical shift, and p is the relative peak position for each species. In the formula, the AFA-PLN chemical shifts corresponded to 0, and pS16-AFA-PLN to 1. The HN NOE value was calculated as an average of HN NOE values for all residues in domain Ia, loop, and domain Ib (residues 2–31). To determine the normalized solvent exchange, we measured peak intensities from [^{1}H,^{15}N] SEA-CLEANEX spectra using the software Sparky.[55] The intensities were corrected for the differences in sensitivity for residues in a [^{1}H–^{15}N] HSQC spectrum and were then normalized among the different PLN species (AFA-PLN, pS16-AFA-PLN, S16D-AFA-PLN, and S16E-AFA-PLN) by assuming Glu2 to have the same solvent exchange for all mutants. The averaged normalized solvent exchange value included residues in domain Ia, loop, and domain Ib (2–30). Residues 15–17 were excluded from the analysis due to their proximity to the phosphorylated/mutated Ser16, and residues 5, 9, and 25 were removed due to spectral overlap.

Supplementary Data

Supplementary data associated with this article can be found, in the online version, at doi:10.1016/j.jmb.2011.03.015

References

1. Simmerman, H. K., Collins, J. H., Theibert, J. L., Wegener, A. D. & Jones, L. R. (1986). Sequence analysis of phospholamban. Identification of phosphorylation sites and two major structural domains. *J. Biol. Chem.* **261**, 13333–13341.
2. Reddy, L. G., Jones, L. R. & Thomas, D. D. (1999). Depolymerization of phospholamban in the presence of calcium pump: a fluorescence energy transfer study. *Biochemistry*, **38**, 3954–3962.
3. Tada, M. & Kadoma, M. (1989). Regulation of the Ca^{2+} pump ATPase by cAMP-dependent phosphorylation of phospholamban. *BioEssays*, **10**, 157–163.
4. MacLennan, D. H. & Kranias, E. G. (2003). Phospholamban: a crucial regulator of cardiac contractility. *Nat. Rev., Mol. Cell Biol.* **4**, 566–577.
5. Stokes, D. L. & Green, N. M. (1990). Three-dimensional crystals of CaATPase from sarcoplasmic reticulum. Symmetry and molecular packing. *Biophys. J.* **57**, 1–14.
6. Toyoshima, C., Nakasako, M., Nomura, H. & Ogawa, H. (2000). Crystal structure of the calcium pump of sarcoplasmic reticulum at 2.6 Å resolution. *Nature*, **405**, 647–655.
7. Toyoshima, C. & Nomura, H. (2002). Structural changes in the calcium pump accompanying the dissociation of calcium. *Nature*, **418**, 605–611.
8. Sorensen, T. L., Moller, J. V. & Nissen, P. (2004). Phosphoryl transfer and calcium ion occlusion in the calcium pump. *Science*, **304**, 1672–1675.
9. Olesen, C., Sorensen, T. L., Nielsen, R. C., Moller, J. V. & Nissen, P. (2004). Dephosphorylation of the calcium pump coupled to counterion occlusion. *Science*, **306**, 2251–2255.
10. Stokes, D. L., Pomfret, A. J., Rice, W. J., Glaves, J. P. & Young, H. S. (2006). Interactions between Ca^{2+}-ATPase and the pentameric form of phospholamban in two-dimensional co-crystals. *Biophys. J.* **90**, 4213–4223.
11. Young, H. S., Jones, L. R. & Stokes, D. L. (2001). Locating phospholamban in co-crystals with Ca^{2+}-ATPase by cryoelectron microscopy. *Biophys. J.* **81**, 884–894.
12. Seidel, K., Andronesi, O. C., Krebs, J., Griesinger, C., Young, H. S., Becker, S. & Baldus, M. (2008). Structural

characterization of Ca^{2+}-ATPase-bound phospholamban in lipid bilayers by solid-state nuclear magnetic resonance (NMR) spectroscopy. *Biochemistry*, **47**, 4369–4376.

13. Schmitt, J. P., Ahmad, F., Lorenz, K., Hein, L., Schulz, S., Asahi, M. *et al.* (2009). Alterations of phospholamban function can exhibit cardiotoxic effects independent of excessive sarcoplasmic reticulum Ca^{2+}-ATPase inhibition. *Circulation*, **119**, 436–444.

14. Cornea, R. L., Jones, L. R., Autry, J. M. & Thomas, D. D. (1997). Mutation and phosphorylation change the oligomeric structure of phospholamban in lipid bilayers. *Biochemistry*, **36**, 2960–2967.

15. Zamoon, J., Mascioni, A., Thomas, D. D. & Veglia, G. (2003). NMR solution structure and topological orientation of monomeric phospholamban in dodecylphosphocholine micelles. *Biophys. J.* **85**, 2589–2598.

16. Traaseth, N. J., Ha, K. N., Verardi, R., Shi, L., Buffy, J. J., Masterson, L. R. & Veglia, G. (2008). Structural and dynamic basis of phospholamban and sarcolipin inhibition of Ca^{2+}-ATPase. *Biochemistry*, **47**, 3–13.

17. Traaseth, N. J., Shi, L., Verardi, R., Mullen, D. G., Barany, G. & Veglia, G. (2009). Structure and topology of monomeric phospholamban in lipid membranes determined by a hybrid solution and solid-state NMR approach. *Proc. Natl Acad. Sci. USA*, **106**, 10165–10170.

18. Mascioni, A., Karim, C., Zamoon, J., Thomas, D. D. & Veglia, G. (2002). Solid-state NMR and rigid body molecular dynamics to determine domain orientations of monomeric phospholamban. *J. Am. Chem. Soc.* **124**, 9392–9393.

19. Metcalfe, E. E., Zamoon, J., Thomas, D. D. & Veglia, G. (2004). $H/^{15}N$ heteronuclear NMR spectroscopy shows four dynamic domains for phospholamban reconstituted in dodecylphosphocholine micelles. *Biophys. J.* **87**, 1205–1214.

20. Zamoon, J., Nitu, F., Karim, C., Thomas, D. D. & Veglia, G. (2005). Mapping the interaction surface of a membrane protein: unveiling the conformational switch of phospholamban in calcium pump regulation. *Proc. Natl Acad. Sci. USA*, **102**, 4747–4752.

21. Karim, C. B., Zhang, Z., Howard, E. C., Torgersen, K. D. & Thomas, D. D. (2006). Phosphorylation-dependent conformational switch in spin-labeled phospholamban bound to SERCA. *J. Mol. Biol.* **358**, 1032–1040.

22. Nesmelov, Y. E., Karim, C. B., Song, L., Fajer, P. G. & Thomas, D. D. (2007). Rotational dynamics of phospholamban determined by multifrequency electron paramagnetic resonance. *Biophys. J.* **93**, 2805–2812.

23. Metcalfe, E. E., Traaseth, N. J. & Veglia, G. (2005). Serine 16 phosphorylation induces an order-to-disorder transition in monomeric phospholamban. *Biochemistry*, **44**, 4386–4396.

24. Traaseth, N. J., Thomas, D. D. & Veglia, G. (2006). Effects of Ser16 phosphorylation on the allosteric transitions of phospholamban/Ca^{2+}-ATPase complex. *J. Mol. Biol.* **358**, 1041–1050.

25. Hughes, E., Clayton, J. C. & Middleton, D. A. (2009). Cytoplasmic residues of phospholamban interact with membrane surfaces in the presence of SERCA: a new role for phospholipids in the regulation of cardiac calcium cycling? *Biochim. Biophys. Acta*, **1788**, 559–566.

26. Abu-Baker, S. & Lorigan, G. A. (2006). Phospholamban and its phosphorylated form interact differently with lipid bilayers: a ^{31}P, ^{2}H, and ^{13}C solid-state NMR spectroscopic study. *Biochemistry*, **45**, 13312–13322.

27. Chu, S., Abu-Baker, S., Lu, J. & Lorigan, G. A. (2010). N Solid-state NMR spectroscopic studies on phospholamban at its phosphorylated form at ser-16 in aligned phospholipid bilayers. *Biochim. Biophys. Acta*, **1798**, 312–317.

28. Wegener, A. D., Simmerman, H. K., Lindemann, J. P. & Jones, L. R. (1989). Phospholamban phosphorylation in intact ventricles. Phosphorylation of serine 16 and threonine 17 in response to β-adrenergic stimulation. *J. Biol. Chem.* **264**, 11468–11474.

29. Ha, K. N., Traaseth, N. J., Verardi, R., Zamoon, J., Cembran, A., Karim, C. B. *et al.* (2007). Controlling the inhibition of the sarcoplasmic Ca^{2+}-ATPase by tuning phospholamban structural dynamics. *J. Biol. Chem.* **282**, 37205–37214.

30. Hoshijima, M., Ikeda, Y., Iwanaga, Y., Minamisawa, S., Date, M. O., Gu, Y. *et al.* (2002). Chronic suppression of heart-failure progression by a pseudophosphorylated mutant of phospholamban via *in vivo* cardiac rAAV gene delivery. *Nat. Med.* **8**, 864–871.

31. Karim, C. B., Marquardt, C. G., Stamm, J. D., Barany, G. & Thomas, D. D. (2000). Synthetic null-cysteine phospholamban analogue and the corresponding transmembrane domain inhibit the Ca-ATPase. *Biochemistry*, **39**, 10892–10897.

32. Clayton, J. C., Hughes, E. & Middleton, D. A. (2005). Spectroscopic studies of phospholamban variants in phospholipid bilayers. *Biochem. Soc. Trans.* **33**, 913–915.

33. Lockwood, N. A., Tu, R. S., Zhang, Z., Tirrell, M. V., Thomas, D. D. & Karim, C. B. (2003). Structure and function of integral membrane protein domains resolved by peptide-amphiphiles: application to phospholamban. *Biopolymers*, **69**, 283–292.

34. Hubbard, J. A., MacLachlan, L. K., Meenan, E., Salter, C. J., Reid, D. G., Lahouratate, P. *et al.* (1994). Conformation of the cytoplasmic domain of phospholamban by NMR and CD. *Mol. Membr. Biol.* **11**, 263–269.

35. Huggins, J. P. & England, P. J. (1987). Evidence for a phosphorylation-induced conformational change in phospholamban from the effects of three proteases. *FEBS Lett.* **217**, 32–36.

36. Ladokhin, A. S. & White, S. H. (1999). Folding of amphipathic α-helices on membranes: energetics of helix formation by melittin. *J. Mol. Biol.* **285**, 1363–1369, doi:10.1006/jmbi..1998.2346.

37. White, S. H. & Wimley, W. C. (1999). Membrane protein folding and stability: physical principles. *Annu. Rev. Biophys. Biomol. Struct.* **28**, 319–365.

38. Fersht, A. (1999). *Structure and Mechanism in Protein Science.* W. H. Freeman & Co., New York, NY.

39. D'Onofrio, M., Ragona, L., Fessas, D., Signorelli, M., Ugolini, R., Pedo, M. *et al.* (2009). NMR unfolding studies on a liver bile acid binding protein reveal a global two-state unfolding and localized singular behaviors. *Arch. Biochem. Biophys.* **481**, 21–29.

40. Zhang, H., Neal, S. & Wishart, D. S. (2003). RefDB: a database of uniformly referenced protein chemical shifts. *J. Biomol. NMR*, **25**, 173–195.

41. Li, P., Martins, I. R., Amarasinghe, G. K. & Rosen, M. K. (2008). Internal dynamics control activation and activity of the autoinhibited Vav DH domain. *Nat. Struct. Mol. Biol.* **15**, 613–618.

42. Traaseth, N. J. & Veglia, G. (2010). Probing excited states and activation energy for the integral membrane protein phospholamban by NMR CPMG relaxation dispersion experiments. *Biochim. Biophys. Acta*, **1798**, 77–81.

43. MacLennan, D. H., Kimura, Y. & Toyofuku, T. (1998). Sites of regulatory interaction between calcium ATPases and phospholamban. *Ann. N. Y. Acad. Sci.* **853**, 31–42.

44. Andronesi, O. C., Becker, S., Seidel, K., Heise, H., Young, H. S. & Baldus, M. (2005). Determination of membrane protein structure and dynamics by magic-angle-spinning solid-state NMR spectroscopy. *J. Am. Chem. Soc.* **127**, 12965–12974.

45. Stevenson, L. W. (2003). Clinical use of inotropic therapy for heart failure: looking backward or forward? Part II: chronic inotropic therapy. *Circulation*, **108**, 492–497.

46. Wright, P. E. & Dyson, H. J. (2009). Linking folding and binding. *Curr. Opin. Struct. Biol.* **19**, 31–38.

47. Mittag, T., Kay, L. E. & Forman-Kay, J. D. (2009). Protein dynamics and conformational disorder in molecular recognition. *J. Mol. Recognit.* **23**, 105–116.

48. Yao, X., Rosen, M. K. & Gardner, K. H. (2008). Estimation of the available free energy in a LOV2-Jα photoswitch. *Nat. Chem. Biol.* **4**, 491–497.

49. Buck, B., Zamoon, J., Kirby, T. L., DeSilva, T. M.., Karim, C., Thomas, D. & Veglia, G. (2003). Overexpression, purification, and characterization of recombinant Ca-ATPase regulators for high-resolution solution and solid-state NMR studies. *Protein Expr. Purif.* **30**, 253–261.

50. Masterson, L. R., Bortone, N., Yu, T., Ha, K. N., Gaffarogullari, E. C., Nguyen, O. & Veglia, G. (2009). Expression and purification of isotopically labeled peptide inhibitors and substrates of cAMP-dependant protein kinase A for NMR analysis. *Protein Expression Purif.* **64**, 231–236.

51. Yonemoto, W. M., McGlone, M. L., Slice, L. W. & Taylor, S. S. (1991). Prokaryotic expression of catalytic subunit of adenosine cyclic monophosphate-dependent protein kinase. *Methods Enzymol.* **200**, 581–596.

52. Masterson, L. R., Mascioni, A., Traaseth, N. J., Taylor, S. S. & Veglia, G. (2008). Allosteric cooperativity in protein kinase A. *Proc. Natl Acad. Sci. USA*, **105**, 506–511.

53. Reddy, L. G., Cornea, R. L., Winters, D. L., McKenna, E. & Thomas, D. D. (2003). Defining the molecular components of calcium transport regulation in a reconstituted membrane system. *Biochemistry*, **42**, 4585–4592.

54. Karim, C. B., Kirby, T. L., Zhang, Z., Nesmelov, Y. & Thomas, D. D. (2004). Phospholamban structural dynamics in lipid bilayers probed by a spin label rigidly coupled to the peptide backbone. *Proc. Natl Acad. Sci. USA*, **101**, 14437–14442.

55. Delaglio, F., Grzesiek, S., Vuister, G. W., Zhu, G., Pfeifer, J. & Bax, A. (1995). NMRPipe: a multidimensional spectral processing system based on UNIX pipes. *J. Biomol. NMR*, **6**, 277–293.

56. Goddard, T. D. & Kneller, D. G. (1999). SPARKY 3.

57. Kay, L. E., Keifer, E. & Saarinen, T. (1992). Pure absorption gradient enhanced heteronuclear single quantum correlation spectroscopy with improved sensitivity. *J. Am. Chem. Soc.* **114**, 10663–10665.

58. Farrow, N. A., Muhandiram, R., Singer, A. U., Pascal, S. M., Kay, C. M., Gish, G. *et al.* (1994). Backbone dynamics of a free and phosphopeptide-complexed Src homology 2 domain studied by ^{15}N NMR relaxation. *Biochemistry*, **33**, 5984–6003.

59. Lin, D., Sze, K. H., Cui, Y. & Zhu, G. (2002). Clean SEA-HSQC: a method to map solvent exposed amides in large non-deuterated proteins with gradient-enhanced HSQC. *J. Biomol. NMR*, **23**, 317–322.

60. Mori, S., Berg, J. M. & van Zijl, P. C. (1996). Separation of intramolecular NOE and exchange peaks in water exchange spectroscopy using spin-echo filters. *J. Biomol. NMR*, **7**, 77–82.

61. Hwang, T. L., van Zijl, P. C. & Mori, S. (1998). Accurate quantitation of water–amide proton exchange rates using the phase-modulated CLEAN chemical EXchange (CLEANEX-PM) approach with a Fast-HSQC (FHSQC) detection scheme. *J. Biomol. NMR*, **11**, 221–226.